Title

BRITTLE FRACTURE IN FILAMENT-REINFORCED MATERIALS

Author

Kerhuel, Guillaume Robert.

Publication Date

1971-09-01

Thesis/dissertation

BRITTLE FRACTURE IN FILAMENT-REINFORCED MATERIALS

Guillaume Robert Kerhuel
(M.S. Thesis)

September 1971

AEC Contract No. W-7405-eng-48

DISCLAIMER

Table of Content

Knowledge is proud that he has learned so much.

Wisdom is humble, that he knows no more.

William Cowper

(Winter Walk at Noon)

BRITTLE FRACTURE IN FILAMENT-REINFORCED MATERIALS

Guillaume Robert Kerhuel

Inorganic Materials Research Division, Lawrence Berkeley Laboratory and Department of Materials Science and Engineering, College of Engineering; University of California, Berkeley, California

ABSTRACT

The fracture behavior of boron-aluminum was investigated. Monolayer tapes of boron fibers imbedded in an aluminum matrix by a liquid infiltration process were tested in simple tension at room temperature. It was repeatedly observed that the entire gage length of the specimen shatters at fracture, and a series of parallel fractures was obtained.

The number of broken fibers within the composite was measured at different stress levels and in the broken parts of the specimen. In all cases this number was found to be very small. The fracture distribution along the gage length did not show any symmetry but was not random. In all cases long and short broken parts were obtained. Examination of the fracture surfaces showed typical features related to the length of the broken part examined. Though few experimental results are available at the present time, it is believed that "secondary" fractures result from local compression due to dispersion of stress-waves emitted during the first or "initial" fracture. The phenomenon observed depends not only on the material investigated but also on the geometry of the tensile specimen. It is similar to Hopkinson multiple fractures phenomenon and should be observable with other brittle elastic and dispersive material.

LIST OF NOTATION

a, b	adjustable parameters in the approximation of Weibull's distribution function.
c	subscript, refer to the composite
c_b	bar velocity, also phase velocity for infinite wavelength
cov	coefficient of variation
d_f	fiber diameter
E	Young's modulus
f	subscript, refers to the fibers
I	moment of inertia
K	stress concentration coefficient
K_m	strength coefficient of the matrix
l	composite thickness
L	composite width
l_o	length submitted to compressive stresses
m	adjustable Weibull's coefficient
m	subscript, refers to the matrix
n	number of fibers in the composite
n_m	strain hardening coefficient of the matrix
N_b	number of breaks per unit length for the composite.
p	step-pressure load at compressive wave emission.
P_{cr}	Euler's load for instability in compression
s	standard deviation
S_c	cross-section of the composite
UTS	subscript, refers to ultimate tensile strength
$\dot{u}$	particle velocity

v volume fraction

Y subscript, refers to yielding

$-$ upperline, refer to mean value

ε strain

$\dot{\varepsilon}$ strain rate

ρ density

σ stress

σ_{θ} adjustable Weibull's coefficient

σ_1 stress in the fibers within the composite when no fibers are broken.

σ_2 stress in the fibers distant from the only broken fiber within the composite.

$\sigma_{2'}$ stress in the two fiber neighboring the only broken fiber within the composite

σ_b bundle strength.

σ_u adjustable Weibull's coefficient

I. INTRODUCTION

The study and development of composite materials has been largely motivated by structural applications. Current developments are pointed towards combinations of unusually strong, high-modulus fibers and organic, ceramic or metal matrices. The successful development of glass-epoxy and boron-epoxy composites has verified approximate theories and provided the technology from which composite structures can be designed that show high strength-to-weight ratio and high modulus-to-weight ratio. Aerospace technology requirements for high strength at slightly elevated temperature for a material of low density suggested the use of aluminum or an aluminum alloy as matrix material. As a result aluminum matrices reinforced with boron fibers are now available on the market.

In order to utilize fully the strength of these materials, consideration of their fracture behavior is necessary. H. T. Corten[1] presented a survey of fracture mechanisms and provided an abundant bibliography. Also Tetelmann[2] has given a general review of fracture in fiber composite materials which presents some theoretical concepts for crack propagation. However, the fracture behavior of the material investigated in this study differs from that usually observed in that the entire gage length of the specimen shatters at fracture. The material contains boron fibers as will be described later. It has been observed that boron fibers tested in simple tension shatter frequently, this being characteristic of high strength brittle materials releasing stored elastic energy at fracture.[3] No experimental data could be obtained on such fracture behavior, and the mechanism of secondary fractures is still unclear. In the course of this study,

it was deemed desirable to investigate the reason why this particular composite tape shows the same fracture behavior as that of boron fibers.

This study is composed of three parts. In the first one, the stress-strain curves of the fibers and of the material were investigated. In the second part, the mechanism of "secondary" fractures was analysed. A tentative explanation is then given.

II. MATERIAL DESCRIPTION

The material whose fracture behavior was investigated is a monolayer tape made of an aluminum matrix reinforced with boron fibers ("Nitroboral"). Figures 1 and 2 show polished cross-sections of such a tape. The fiber diameter is $d_f = 140\mu = 5.5$ mils. The width of the tape is $L = 85$ mils and its thickness $l = 9$ mils. The surface of the material was not plane but presented several waves due to the fibers. Therefore the cross-sections S_c of a specimen was less than $9 \times 10^{-3} \times 85 \times 10^{-3} = 7.65 \times 10^{-4}$ in^2. Furthermore it was not constant along the gage length of a tensile specimen. Fortunately the aluminum matrix carried only a small fraction of the load at fracture and variations in the cross-section area of the matrix did not affect the fracture behavior significantly. An average value of $S_c = 7.2 \times 10^{-4}$ in^2 was found to be in agreement with most results, the standard deviation being 0.4×10^{-4} in^2.

The tape contained $n = 16$ parallel fibers. Since $16\ d_f$ (= 88 mils) is greater than the width of the tape $L = 85$ mils it is seen that all fibers are not exactly in the same plane, as can be seen on Fig. 2. The average distance between neighboring fibers is about 3μ. The fiber volume fraction v_f is very close to 50% and is considered equal to that value in the following calculation.

The matrix was an aluminum alloy whose nominal composition, as stated by the manufacturer was

3.7/5.5 Cu
0.4/1.2 Ag
0.2/0.8 Mn
0.2/0.6 Mg

0.03/0.035 Ti
0.15 Si
0.15 Fe

According to the manufacturer its Young's modulus is 10×10^6 psi, its tensile strength 72,000 psi. The boron fibers were made by vapor deposition of boron on a tungsten wire. The composite tape was made by a continuous liquid infiltration process. A submicron boron nitride coating of the fibers applied just prior to the metal infiltration process but also as part of the continuous fabrication prevented chemical degradation of the fibers during liquid infiltration[4,5] and provides an excellent mechanical bonding at the filament-matrix interface. This composite material was manufactured by the Monjoe Scientific Corporation (Palo Alto).

III. STRESS-STRAIN CURVES AND INITIAL FRACTURE

A. Mechanical Properties of the Fibers

Fibers obtained through etching away the Al alloy matrix of the composite in 10% NaOH were tested in simple tension. No test was made with as produced fibers. It is claimed[6,7] that 15-25% reductions in fiber tensile strength result from this etching process. This was attributed to defects introduced on the surface of the fibers during etching rather than to degradation of the fibers during fabrication. In the present case, such reductions were limited since the fibers tested showed high tensile strengths, only slightly lower than those of as-produced boron fibers as reported by the manufacturer. Their Young's modulus was, however, 22% lower than what was expected, but was consistent with the Young's modulus measured for the composite, and predicted by the rule of mixtures.

Testing was performed by epoxy-bonding grooved aluminum tabs to the filament ends. A standard gage length of 2 inches was used. Fig. 3 shows a typical stress-strain curve. Figure 4 shows the cumulative frequency distribution of strength and the Weibull's distribution that has been associated:

$$F(\sigma) = 1 - \exp\left(-\left(\frac{\sigma - 320}{120}\right)^{3.5}\right)$$

σ in 10^3 psi.

$F(\sigma)$ is the probability that a value less than σ will be obtained.[8] The number of test conducted was not sufficient for a χ^2 test of significance to be done but experimental and theoretical curves coincide and the experimental values are found in agreement with those

calculated according to the following formula:

Weibull's function:

$$F(\sigma) = 1 - \exp\left(-\left(\frac{\sigma - \sigma_u}{\sigma_o}\right)^m\right) \qquad (1)$$

average value:

$$\bar{\sigma} = \sigma_o\,\Gamma\left(\frac{m+1}{m}\right) + \sigma_u \qquad (2)$$

standard deviation:

$$s = \sigma_o \sqrt{\Gamma\left(\frac{m+2}{m}\right) - \Gamma^2\left(\frac{m+1}{m}\right)} \qquad (3)$$

coefficient of variation: $cov = \frac{s}{\bar{\sigma}}$

where Γ is the tabulated gamma function.

The Weibull's function was introduced experimentally based on comparison with extensive experimental data. Thus while physical interpretation can be assigned to σ_o and σ_u, no theoretical foundation can be provided for these interpretations. In fact, they are extrapolations of an empirical function from a region that can be investigated experimentally into a region that cannot be investigated experimentally. Thus further speculation concerning physical interpretation of σ_o and σ_u appears unwarranted. The following results were obtained:

	experimental	calculated
$\bar{\sigma}$	440,000 psi	432,000 psi
s_f	40,000 psi	39,500 psi
cov	9%	9.1%

For as-produced fibers, only 10% of the fibers have tensile strength less than 450,000 psi.

The average Young's modulus is 48.1×10^6 psi, compared to 60×10^6 psi claimed by the manufacturer, with a standard deviation of 1.2×10^6 psi (cov = 2.5%). A change in slope is usually observed at a stress level about 340,000 psi ($\varepsilon_f = 0.7\%$). The stress-strain curve is then almost linear, but the values of the slope (average value 41×10^6 psi) are more scattered (standard deviation 3.6×10^6 psi, cov = 9%). Finally it was found that fibers obtained from the broken parts of specimen tested at fracture show the higher tensile strength and the lower values of the Young's modulus. At fracture, the specimens shatter into many pieces.

B. Composite Stress-Strain Curve:

Figure 5 shows tensile test specimens. Tabs have not been epoxied at one end of one of these specimens. In the middle of the picture are broken parts of a specimen tested at fracture. Figure 3 shows a typical stress-strain curve obtained. Figure 4 shows the cumulative frequency distribution of strength and the Weibull's distribution that has been associated:

$$F(\sigma) = 1 - \exp\left(- \left(\frac{\sigma - 85}{73}\right)^3 \right)$$

σ in 10^3 psi

The following results were obtained:

	experimental	calculated
$\bar{\sigma}_c$	157,000 psi	154,000 psi
s_c	23,000 psi	22,850 psi
cov	15%	14.8%

The first two stages of the composite stress-strain curve, as suggested by McDanels, Jech and Weeton[9] were observed, namely:

I) Elastic deformation of both fibers and matrix from $\sigma_c = 0$ to $\sigma_c = 91{,}000$ psi ($\varepsilon_c = 0.33\%$).

II) Elastic fiber deformation but plastic deformation of the matrix from $\sigma_c = 91{,}000$ psi to $\sigma_c = 157{,}000$ psi ($\varepsilon_c = 0.58\%$).

The average Young's modulus for stage I is $\bar{E}_c = 27.6 \times 10^6$ psi (standard deviation 0.7×10^6 psi cov = 2.6%).

According to a popular, emperical, and naive rule of mixtures

$$E_c = E_f v_f + E_m v_m$$

where $E_m = 10 \times 10^6$ psi, $E_f = 48.1 \times 10^6$ psi and $v_m = v_f = 0.5$,
Thus in this cae $E_c = 29 \times 10^6$ psi

This rule implies a very good bonding between the matrix and the fibers so that a plane cross-section of the specimen remains plane during loading. Elongations are thus the same for all points on the cross-section. It assumes furthermore a uniform distribution of stresses in the fiber material as well as in the matrix material. This assumption is not valid at the ends of the specimen and in cross-sections where the fiber modulus is not the same for all fibers. Rigorous calculation of the modulus involves consideration of the statistical distribution of elastic modulus of the fibers and of the geometry of the composite which is critical in the present case of a monolayer tape, the rule of mixtures providing only an upper bound for the modulus of the composite.[1] Experimental results are found in agreement with the above considerations.

For stage II, the rule of mixtures gives:

$$\sigma_c = \sigma_f v_f + \sigma_{mY} v_m$$

since $v_f = 0.5$, and assuming $\varepsilon_c = \varepsilon_m = \varepsilon_f$ and

$$\sigma_{mY} = K_m \varepsilon_m^{n_m}, \quad E_c = 0.5 \; (E_f + K_m \varepsilon_m^{n_m - 1})$$

K_m being the strength coefficient (about 50,000 psi) and n_m the strain hardening coefficient (about 0.1). With these values, $E_c = 25.5 \times 10^6$ psi.

Composite stress-strain curves were not determined with enough accuracy to allow calculation of K_m and n_m. Such calcualtions must be made on the matrix material itself. In the present case, stage II is assimilated to a straight line with an average slope of 26.1 10^6 psi, in agreement with the value calculated above, the coefficient of variation being about 8%.

C. Initial Fracture:

Rosen in "The Strength and Stiffness of Fibrous Composites"[10] presents a general analysis of failure mechanisms, and provides an abundant bibliography. The statistical model, based on an accumulation of fiber failures[11] is an analytical method which has many advantages over the popular rule of mixtures approach. In connection with the coupled failure-mode problem, it is interesting to note that the statistical tensile-failure model can be used to provide insight into the stress-concentration effect; that is, it is possible to account for a nonuniform redistribution of the load which has been carried in the filament before it has broken. For example it is assumed that for every broken fiber, there are two adjacent fibers

which carry a stress equal to a multiple K, the stress-concentration coefficient, of the stress carried in the other fibers.[12,13,14] Assuming a linear cumulative distribution function for the fiber strength, a computation was made that shows the effects of the stress-concentration coefficient on the fraction of fibers fractured before failure of the composite and on the average failure stress. Results of this calculation are reported in.[10]

In the present case, the distribution function for fiber strength can be represented by:

$$F_1(\sigma) = \frac{\sigma_1 - a}{b - a} \tag{4}$$

where b = 485,000 psi

a = 390,000 psi

If σ is the average stress in the composite, σ_1 the stress carried by the fibers within the composite when no fiber is broken ($\sigma_1 = \frac{\sigma - \sigma_m (1 - v_f)}{v_f}$), σ_2' the stress carried by the two fibers next to the only broken fiber within the composite, and σ_2 the stress carried by the other fibers when only one fiber has failed ($\sigma_2' = K\,\sigma_2$): After the first fiber has failed, the stress distribution is given by:

$$n\sigma_1 = 2K\sigma_2 + (n-1-2)\,\sigma_2 \tag{5}$$

n being the number of fibers (16 fibers) in the composite.

$$\sigma_2 = \frac{n}{2K + n - 3}\,\sigma_1 \tag{6}$$

The probability for failure of a fiber next to the only broken fiber is:

$$F_{2'}(\sigma) = \frac{\frac{Kn}{2K + n - 3}\sigma_1 - a}{b - a} \tag{7}$$

and the probability for failure of another fiber is:

$$F_2(\sigma) = \frac{\frac{n}{2K + n - 3}\sigma_1 - a}{b - a} \tag{8}$$

Since K is always greater than 1, $F_{2'}(\sigma)$ is always greater than $F_1(\sigma)$. The probability for at least one secondary failure is:

$$\frac{n - 3}{n - 1} F_2(\sigma) + \frac{2}{n - 1} F_{2'}(\sigma)$$

Figure 6 represents $F_1(\sigma)$, $F_2(\sigma)$ and $F_{2'}(\sigma)$ for K = 1.2 and K = 1.4. For example for K = 1.2 and σ_1 = 400,000 psi:

$$F_1(\sigma) = 0.105$$

$$F_2(\sigma) = 0.27$$

$F_{2'}(\sigma) = 1.14$, greater than 1.

In these circumstances, failure of the first fiber leads to failure of the neighboring fibers since $F_{2'}(\sigma)$ is greater than 1 and therefore leads to failure of the composite. In general for:

$$\frac{Kn}{2K + n - 3} > \frac{b}{a}$$

or (10)

$$K > \frac{n - 3}{\frac{a}{b} n - 2}$$

this failure mode always occurs:

(10) leads to: $$\frac{Kn\sigma_1}{2K + n - 3} > b\frac{\sigma_1}{a} \tag{11}$$

since the first failure occurs at $\sigma_1 > a$,

(11) and (7) leads to $F_{2'}(\sigma) > 1$

In the present case, n = 16, a = 390,000 psi and b = 485,000 psi.

$$\frac{n - 3}{\frac{a}{b} n - 2} = 1.2$$

It is seen at the same time that the number of fibers fractured before failure of the composite is theoretically zero.

The scatter in strength of the fibers, measured by the Weibull m-parameter, gives a ratio of bundle strength to average fiber strength of 0.6,[1] the bundle strength being then about 265,000 psi. This ratio is determined according to the bundle theory where assuming $\sigma_u = 0$,

$$\frac{\sigma_b}{\sigma_f} = \frac{(me)^{-1/m}}{\Gamma(\frac{m + 1}{m})} \tag{12}$$

This value is to be used in the rule of mixtures. The rule of mixture can be applied in the present case of fracture according to a crack propagation mode rather than to a statistical accumulation of fiber failures.

$$\begin{aligned}\sigma_{cUTS} &= \sigma_f v_f + \sigma_{mY} v_m \\ &= (265,000 + 60,000)\ 0.5 \\ &= 162,000 \text{ psi}\end{aligned}$$

This value is in agreement with the experimental result:

$$\sigma_{cUTS} = 157,000 \text{ psi}$$

D. Conclusion

The stress-strain curve of the material and the fracture mode of the initial fracture have been investigated. Results are found in agreement with recent theories. Due to the geometry of the material and the small number of reinforcing fibers, a high stress-concentration coefficient causes crack propagation and failure of the composite as soon as one fiber breaks. This is also evidenced by the very small number of fibers fractured prior to composite failure. This will be discussed in the next section.

IV. SECONDARY FRACTURES RELATION WITH STRESS WAVES:

Secondary fractures were not observed with a specimen made of the same material, but three times as wide; they are therefore related to the geometry of the specimen and not only to its nature. Such secondary fractures should be obtainable with another similar material, if the geometry of the tensile specimen is the proper one.

The phenomenon of one secondary fracture was described by Micklowitz[15] in terms of elastic wave propagation. Phillips developed this concept and associated flexural pulses with Timoshenko beam theory.[16] Achenbach and Nuismer provided a theory relating instantaneous crack propagation to energy balance.[17] In 1912, Bertram Hopkinson[18] discovered the phenomenon known as "spalling" or "scabbing" that produces a serie of parallel Hopkinson fractures. However, to the author's knowledge, no paper was published dealing with fracture density as high as 4.5 fractures per inch.

In order to estimate the effect of wave propagation, tests were run that allowed investigation of the distribution of fractures along the gage length of the tensile specimens. Such tests, however, would not have been significant without prior annalysis of fiber breakage before failure of the composite.

A. Fiber Breakage Prior to Composite Failure:

Four inches long specimens were loaded at stress levels reported in Table I. The load was kept for five minutes and removed at the same strain rate

Table I. Stress levels

number of tests	strain rate	stress level
2	3.3×10^{-5} sec^{-1}	90,000 psi
2	3.3×10^{-5}	120,000
2	3.3×10^{-5}	150,000
1	3.3×10^{-4}	90,000
1	3.3×10^{-4}	120,000
1	3.3×10^{-4}	150,000

One additional specimen was loaded up to 180,000 psi. Among all the specimens tested at fracture, none failed at stresses lower than 90,000 psi, 8% at stresses lower than 120,000 psi, 38% at stresses lower than 150,000 psi and 85% at stresses lower than 180,000 psi.

The accoustic waves emitted during the tests were recorded, using the method suggested by Mehan and Mullin.[19] The specimens were then submitted to high resolution radiographic inspection. Finally the matrix was etched away so that the fibers could be seen with the naked eye. While details of the first two experimental methods of investigation are questionable, the later is quite reliable.

Accoustic waves are emitted during the loading phase, during the static phase and also during the unloading phase. In some cases, accoustic wave emission was also detected on the stress-strain curve. As was seen later, these waves were not related to fiber failures. They might be due to other factors such as failure of the epoxy bond between the composite tape and the tabs used to transfer the load, or to

vibrations in the Instron testing unit. Thus this method did not provide any definitive information.

Radiographic inspection did not show any break in any of the fibers. Some breaks were, however, discovered later. The reason that these were not observable on the photographic film is that the two fracture surfaces remain too close for a gap to be detected. (Only the tungsten core of the fibers is seen on the film).

Dissolution of the matrix provided better results since the fibers could be seen with the naked eye. Out of 160 fibers investigated, only 5 were found broken. Detailed examination showed that:

1) Dissolution of the matrix in as-produced material did not show any break in any of the fibers.

2) In a specimen stressed at 150,000 psi ($\dot{\varepsilon} = 3.3 \times 10^{-4}$ sec^{-1}), one fiber, on the edge of the tape showed 5 fractures. The length of the broken parts of this fiber were, in mm: 24.5, 37.5, 10.0, 12.9 and 7.0. These broken parts were tested separately. A tensile strength of 275,000 psi was measured (only 63% of the average fiber strength). It is likely that the mechanical properties of this fiber have been degraded during some step of the fabrication or production processes.

3) In a specimen tested at 90,000 psi ($\dot{\varepsilon} = 3.3 \times 10^{-5}$ sec^{-1}), two fibers, in the middle of the tape, were broken. One exhibited a fracture at 34 mm from one end, the other two fractures at 33.8 and 35.9 mm respectively from the same end. Figures 7 and 8 are scanning electron fractographs of the first and the second fiber respectively.

4) The same type of results was obtained with a specimen stressed at 120,000 psi ($\dot{\varepsilon} = 3.3 \times 10^{-4}$ sec^{-1}). Figures 9 and 10 are fractographs of the single fractured fiber and the double fractured fiber respectively.

5) No failure was observed in the specimen stressed at 180,000 psi.

Once one fiber is broken, the neighboring fibers are overloaded in the plane of that break. Using the notation of III. C. the stresses after failure of these fibers are, for K = 1.2:

	σ	$\sigma_1 = \sigma_f$		σ_2	σ_2'
case 1	150,000 psi	258,000 psi		268,000 psi	322,000 psi
case 2	90,000	155,000	and	161,000	193,000
				172,000	206,000
case 3	120,000	206,000	and	214,000	255,000
				237.000	306,000

Since the first fiber failure occured at an effective fiber stress σ_f, much smaller than a = 390,000 psi, the criterion suggested above cannot be applied. The present measurements are concerned with a very small number of fibers (3%) that fail at very low stresses due to defects of fabrication. Therefore they do not lead to failure of the composite as would do 97% of the fibers that would have failed at stresses higher than 390,000 psi.

Figure 2 shows, however, that a stress σ_f = a is not achieved, even at failure of the composite. Such a result emphasises the importance of fiber failure at low stresses, causing composite failure, this being due to the small number of reinforcing fibers and to the high stress-concentration coefficient.

"a" was determined so that the straight line chosen for $F(\sigma)$ represented as closely as possible the fiber strength distribution, for the highest possible number of fibers, regardless of the drastic effect of a weak fiber on the composite strength. A value of "a" determined by extrapolation of experimental results should be preferred in order to apply this criterion. In the present case, a value of a = 300,000 psi is found (Fig. 4). Equation (10) leads then to K = 1.65.

Finally on a theoretical basis it is quite possible to find breaks in the same fiber within 2mm since the nominal stress is shear transmitted in a discontinuous fiber within 0.5mm.

Results obtained by Prewo[3] coincide with the present results in that very few fibers are broken during the loading phase in this type of composite. Therefore a distribution of fiber breaks cannot account for multiple fractures over the entire gage length.

B. Broken Fibers After Composite Failure:

The matrix was dissolved in seven broken parts of several specimens tested at fracture. The length of these broken parts varied from 38 to 51 mm. The same etching process as described above was used.

Out of the 112 fibers investigated, only 5 were found broken. This result is reported in Table II.

Table II. Broken Fibers.

length of specimen	number of breaks	distance from one end
3 cm	1	1.5 cm
5 cm	2	2.5 and 3 cm
5.1 cm	2 in neighboring fibers	1.5 cm

Some fibers were also found broken adjacent to the fracture surface of the composite.

This very small number of broken fibers in broken parts of specimens tested at fracture shows that the phenomenon of multiple fractures is not a consequence of a statistical accumulation of fiber breaks. Figures 11 and 12 are fractographs of these broken fibers. They show the effect of the etching process on the tungsten core of the fibers. This effect is seen to be limited. Figures 7 to 12 show fractures initiated at the fiber-matrix interface. Figure 7 to 10 show unusual aspects of the tungsten core. They are interpreted as defects leading to weak points of the fibers that break at stresses lower than the nominal fiber fracture stress.

C. <u>Fracture Distribution Along Gage Length</u>:

Twelve specimens 4, 8 and 12 inches long were tested at fracture. A color spectrum was painted on the specimens so that the broken parts could be brought together in their proper order after composite failure. Figure 13 shows some typical fracture distributions obtained. The only characteristic common to these fracture patterns was that a small part was rarely isolated between longer parts and that the length of small parts in a group showed little variations. Figure 14 shows the number of breaks per unit length versus the load at fracture. Further experiments are necessary to quantify this relation, nevertheless, it is seen that the number of breaks per unit length increases with the load at fracture. If N_b is the number of breaks per unit and σ the load at fracture,

$$N_b = 0.023\,\sigma - 0.9 \quad (\sigma \text{ in } 10^3 \text{ psi})$$

Extrapolating, $N_b = 1$ for $\sigma = 80{,}000$ psi

$N_b = 0$ for $\sigma = 40{,}000$ psi

D. <u>Fractography</u>:

After having studied micromechanisms of deformation and fracture of the components of the composite, R. C. Jones[20] formulated micro-mechanical models to explain the mechanical behavior of such composites. His analyses provided interpretations for different aspects of the fracture surfaces.

Figures 15, 16 and 17 are scanning electron fractographs that correspond to broken parts 6, 5 and 5.7 cm long respectively. Figures 18 and 19 are fractographs that correspond to broken parts 2 and 5 mm long respectively. Figures 20 to 22 are fractographs that correspond to fractures produced by bending the specimens by hand. In the latter tests, the moment of flexion was constant along the gage length and two or three fractures were usually obtained (in four points bending tests): two fractures were obtained repeatedly, they were located at the inner points of application of the load and therefore were not considered as representative of the materials fracture behavior). Such pictures were obtained repeatedly, regardless of the longitudinal position of the fracture, the changes in appearance being only related to the length of the broken part examined.

Analysis of the fracture surfaces (as to point of initiation, etc.) was difficult since the fracture surfaces observed may just be shattered regions within several microns of the initial fracture plane of the fibers.[3] This difficulty is seen in Figs. 20 and 22. However, Figs. 15 to 17 show many analogies with pictures published in the literature for fracture surfaces of boron-aluminum composites that fail only at one place. It is therefore believed that the first fracture occurred between two long parts. No distinction could be detected between fracture surfaces of long broken parts of the same specimen. Thus the first fracture could not be located definitively.

Figures 23 to 26 show that creacks can propagate longitudinaly in the fibers. Such cracks were observed only in few cases, and corresponded always to short broken parts (less than 1 cm) of a tensile specimen. Usually they were propagating in 3 to 6 neighboring fibers. Fig. 26 show that such creacks, when in a longitudinal plane, perpendicular to the plane of the tape, could lead to longitudinal splitting of the tape without failure at the fiber-matrix interface.

E. Conclusion:

The relation between the number of breaks per unit length and the load at fracture supports the general theory of several fractures due to the release of stored elastic energy. Unfortunately, the fracture surfaces being badly shattered, makes it difficult to quantify surface energies. Furthermore, it was observed that some broken parts (in general short parts) flew off with a high velocity. A certain amount of forward momentum has been trapped between two fractures. Thus a fraction of the stored elastic energy is transferred into kinetic energy. The fracture distribution along the gage length is not random. These are several characteristics related to elastic wave propagation.

V. CALCULATIONS STRESS WAVES PROPAGATION AND DISPERSION

A. Bibliography

Rychnovsky[21] presented a general survey of stress waves in solids and provided an abundant bibliography relative to stress waves in composites. He summarized the following concept of wave dispersion:

To find the elementary solution of the wave equation, two assumptions must be made: that each plane cross section of a bar remains plane during its motion, and that the stresses over a cross section are uniform. Both assumtions are consistent with a long wavelength sinusoidal excitation. The "bar velocity" is then given by $c_b = \sqrt{E/\rho}$ where E is the Young's modulus and ρ the material density. Calculation of the longitudinal vibrational mode of the bar may then be assimilated to a Sturm-Liouville problem that can be solved in terms of a Fourier series once the boundary conditions are defined. But for shorter wavelengths, lateral motion of the bar will result in violation of both assumptions necessary for this solution.

Pochhammer[22] and Chree[23] investigated independently the propagation of sinusoidal waves in cylindrical bars. Their solution show a decrease in longitudinal wave velocity as the wavelength becomes small in comparison to the bar diameter, tending to the Rayleigh surface wave velocity. Nonsinusoidal waves can be studied by determining the Fourier components of the wave, analysing the components separately and superimposing the separate solutions because of the linearity of the governing differential equations. Short wavelength components have lower phase velocities than the long wavelength Fourier components[24] thus resulting in a lenghtening of the total wave and a reduction of its amplitude. The lengthening of the wave is termed "dispersion". After the wave has propagated along the bar, the major wave which is changed to a general sinusoidal shape is followed by a series of lower amplitude, high frequency waves which are also sinusoidal in shape.

Effects of elastic waves impringing on rigid immovable parallel cylinders were considered by Cheng.[25] Equations for multiple bars were developed using acoustic theory of multiple scattering. Constraints on the bars make this analysis of limited use for practical problems. Peck and Gurtmann[26] considered the transient analysis of a laminated composite in which geometric dispersion in a step pulse was considered. The low frequency part of the wave gave the dominant contribution to the long time far field solution. An analysis using this wave is called the "head of the pulse" approximation. It is characterized by a dispersion time parameter τ and depends on the two leading terms in the Taylor series expansion of the phase velocity versus frequency for the first longitudinal wave propagation mode:

$$c = c_b - \alpha\omega^2 + \ldots$$

Comparison of experimental results with the head of the pulse approximation were made by Whittier and Peck.[27] Timing, amplitude and wave shape were predicted within a few percent.

Whittier and Peck used laminated composites made from alternating layers of high and low modulus material, which caused a high degree of geometric dispersion of wave propagating in the composite. They conducted experiments in which waves propagated parallel to the lamination. A step-pressure load (p = 70 psi; rising time about a few

nanoseconds) was uniformely applied over the front face of a flat-plate composite (0.25 inch thick) so that the central portion of the plate responded, for a short time, as if the plate were laterally unbounded. Curves representing a nondimensionnal normalized velocity parameter $\frac{\dot{u}\rho c_b}{p}$ versus time after pulse arrival were measured for thornel-reinforced carbon phenolic and boron-reinforced carbon phenolic composites. They show timing and amplitude of the oscillations in normalized velocity.

B. Application

The shape of these curves suggested a tentative explanation for the secondary fractures observed in this study.[28] Since no experimental data is available for the coefficient α of the Taylor expansion, only a semiquantitative explanation can be given.

The phase velocity for infinite wavelengths is $c_b = \sqrt{\frac{E}{\rho}} =$ 0.35 in/µsec. The average velocity for crack propagation is approximated by $0.4\ c_b$ = 0.14 in/µsec. Assuming that the first fracture is initiated at one edge of the tape, the first fracture occurs in $\frac{85 \times 10^{-3}}{0.14}$ = 0.6 µsec. During that time the unloading (compression) wave has travelled over 0.08 inch along the gage length (only 2% of the total gage length) and is therefore considered as a Heaviside step-pulse with a nominal value $p = \bar{\sigma}_c$ = 157,000 psi (average tensile streng strength of the composite). The stresses produced by this wave are related to the particle velocity by the momentum equation: consider a small element dx, the elastic wave passes through it in time $dt = \frac{dx}{c_b}$, the momentum equation being then:

$$\sigma S_c dt = (\rho S_c dx)\dot{u} \rightarrow \sigma = \rho c_b \dot{u}$$

$$\text{or} \quad \sigma = (\text{normalized velocity}) \times p$$

The shape of the stress pulse is modified in the same way as the shape of the normalized velocity pulse in Whittier and Peck's experiments. The oscillations due to dispersion are reported to reach 1.4, the period of the oscillations being about 0.3μ sec. These values correspond to a peak compressive stress of $1.4\ \bar{\sigma}_c = 220{,}000$ psi and a length $l_o = 0.3c_b = 0.1$ inch along the gage length. Thus at a certain distance from the first fracture, the tensile specimen is not only unloaded but "overunloaded" and a length of $l_o = 0.1$ inch is in a state of compression of $1.3\ \bar{\sigma}_c - \bar{\sigma}_c = 47{,}000$ psi.

Euler's formula for instability of a compressed bar with one built in and one free end gives the critical load:

$$P_{cr} = \frac{\pi^2 EI}{4l_o^2} \qquad \text{and} \qquad \sigma_{cr} = \frac{P_{cr}}{S_c}$$

where E is the Young's modulus of the material and I the moment of inertia ($I = \frac{Il^3}{12} = 5.2 \times 10^{-9}$ in^4), is measured in inches and P_{cr} in pounds. For $l_o = 0.1$ inch, $\sigma_{cr} = 49{,}000$ psi. This critical value (due to the low inertia of the tape) is of the same order of magnitude than the average, local, instantaneous compression stress. Thus it is seen that this compression may be responsible for secondary fractures.

C. Discussion

The results reported by Peck and Gurtmann[26] are obtained through several approximations, and no physical interpretation is given for the peak disturbance. These results are supported by the experiments made by Whittier and Peck.[27] The physical interpretation of the normalized velocity being higher than unity is still unclear.

Approximate calculation of buckling of prismatical bars under the action of distributed axial loads can be found in Tinoshenko (theory of elastic stability). But it is necessary to consider first the time required for the compressed Euler's column to fracture and compare this time with the time during which this column is compressed. Further experimental data are necessary to support the applicability of this failure mode. Furthermore flexural waves have not been considered in the present approximation to the first order. Consideration of the interferences between these and longitudinal waves makes the analysis very complicated, and requires computer calculations.

VI. SUMMARY AND CONCLUSION

Tensile tests were made with a material that presented several distinct fractures at failure. This phenomenon was approached in terms of elastic wave propagation and dispersion. A model was proposed according to which secondary fractures might be due to instability in compression. It requires the material to be brittle, elastic and dispersive, and the geometry of the tensile specimens to allow fracture under low compressive stresses. Several experimental data are still necessary to support this theory. It is believed that the same fracture behavior can be observed with other brittle, elastic and dispersive material, providing that the geometry of the tensile specimen is appropriate.

ACKNOWLEDGEMENTS

The author is deeply appreciative to Professors R. H. Bragg, J. E. Dorn and I. Finnie for serving on his thesis committee. He would like to express his gratitude to Dr. W. W. Gerberich for the advice given during the course of this research and Dr. De Runtz for professional guidance. The author is also grateful to Mr. George Georgakopoulos for assistance in the scanning electron microscopy, Mr. Lee Johnson for metallography, Mr. Donald Krieger for preparation of the tensile specimens, Mrs. Shirley Ashley for manuscript preparation, Mrs Gloria Pelatowski for preparation of the line drawings and Mr. Douglas Kreitz for preparation of the pictures.

This work was supported by the United States Atomic Energy Commission through the Inorganic Materials Research Division of the Lawrence Radiation Laboratory.

REFERENCES

1. Herbert T. Corten, "Micromechanics and Fracture Behavior of Composites," in Modern Composite Materials, edited by L. J. Broutmann and R. H. Krock, Addison-Wesley Pub. Co., 1967.

2. A. S. Tetelmann, "Fracture Processes in Fiber Composite Materials," Materials: Testing and Design, ASTM STP460, February 1969.

3. Karl M. Prewo, United Aircraft Research Laboratories, private communication.

4. J. L. Camahort, "Protective Coating by Surface Nitradation of Boron Filaments," J. Composite Materials, Vol. 2, No. 1, January 1968, 104-112.

5. A. E. Vidoz, J. L. Camahort and F. W. Crossmann, "Development of Nitrided Boron Reinforced Metal Matrix Composites," J. Composite Materials, Vol. 3, April 1969, 254-261.

6. C. G. Ryder, A. E. Vidoz and J. L. Camahort, "Mechanical Properties of Nitrided Boron-Aluminum Composites," J. Composite Materials, Vol. 4, April 1970, 264-272.

7. K. C. Anthony and W. H. Chang, "Mechanical Properties of Al-B Composites," Trans ASM, Vol. 61, 1968, 552.

8. W. Weibull, "A Statistical Distribution Function of Wide Applicability," J. Applied Mechanics, Vol. 18, 1951, 293-297.

9. D. L. Danels, R. W. Jech and J. W. Weeton, "Stress-Strain Behavior of Tungsten Fiber Reinforced Copper Composites," NASA T. N. D-1881, October 1963.

10. B. Walter Rosen, "The Strength and Stiffness of Fibrous Composites," in Modern Composite Materials, op. cit.

11. B. Walter Rosen, "Tensile Failure of Fibrous Composites," AIAA Journal, Vol. 2, No. 11, November 1964, 1985-1991.

12. V. R. Riley, "Fiber/Fiber Interaction," J. Composite Materials, Vol. 2, No. 4, October 1968, 436-446.

13. M. J. Iremonger and W. G. Wood, "Effect of Geometry on Stresses in Discontinuous Composite Materials," J. Strain Analysis, Vol. 4, No. 2, 1969, 121-126.

14. Thomas F. MacLaughlin, "A Photoelastic Analysis of Fiber Discontinuities in Composite Materials," J. Composite Materials, Vol. 2, No. 1, January 1968, 122-130.

15. Julius Micklowitz, "Elastic Waves Created During Tensile Fracture, The Phenomenon of a Second Fracture," J. Applied Mechanics, Vol. 75, March 1953, 122-130.

16. J. W. Phillips, "Stress Pulses Produced During the Fracture of Brittle Tensile Specimens," Int. J. Solid Structures, Vol. 6, 1403-1412, Pergamon Press, 1970.

17. J. D. Achenbach and R. Nuismer, "Fracture Generated by a dilatational Wave," Int. J. Fracture Mechanics, Vol. 7, No. 1, 77-88, Wolfers-Noordhoff Pub. Co., March 1971.

18. B. Hopkinson, Collected Scientific Papers, p. 423, 1912, University Press Cambridge, 1921,.

19. R. L. Mehan and J. V. Mullin, "Analysis of Failure Mechanisms Using Acoustic Emission," J. Composite Materials, Vol. 5, April 1971, 266-269.

20. R. C. Jones, "Fractography of Aluminum-Boron Composites," Materials: Testing and Design, ASTM STP 460, 512-527, February 1969.

21. R. E. Rychnovsky, "Survey of Stress Waves in Solids: Fundamental Principles and Current Developments," Sandia laboratories, SCL-M-70-72, May 1970.

22. L. Pochhammer, "Uber die Fortplanzungsgeschwindigkeiten Schwingungen in einem unbegrenzten isotropen Kreiscylinder," Z. Math. (Crelle), Vol. 81, 1876, 324-336.

23. C. Chree, "Longitudinal Vibrations of a Circular Bar," Quart. J. of Math., Vol. 21, 1886, 287-298.

24. H. Kolsky, "Stress Waves in Solids," Dover Publications, Inc., New York, N. Y. 1963.

25. S. L. Cheng, "Multiple Scattering of Elastic Waves by Parallel Cylinders," J. Applied Mechanics, No. 3, Transactions of the ASME, Vol, 36, Series E, 1969, 523-527.

26. J. C. Peck and G. A. Gurtmann, "Dispersive Pulse Propagation Parallel to the Interface of a Laminated Composite," J. Applied Mechanics, No. 3, Trans. ASME, Vol. 36, Series E, 1969, 479-484.

27. J. S. Whittier and J. C. Peck, "Experiments on Dispersive Pulse Propagation in Laminated Composite and Comparison with Theory," J. Applied Mechanics, No. 3, Trans ASME, Vol. 36, Series E, 1969, 485-490.

28. J. A. De Runtz, Lockheed Missile and Space Co., Palo Alto, private communication.

FIGURE CAPTIONS

Fig. 1 and 2. Polished cross-sections of the material studied.

Fig. 3. Stress-strain curve of fiber and of composite.

Fig. 4. Cumulative frequency distribution of strength for the fibers and for the matrix.

Fig. 5. Tensile test specimens and broken parts.

Fig. 6. Effect of the stress-concentration coefficient on the probability of fiber failures.

Fig. 7 to 10 Fiber failure within the composite and without composite failure:

7. = 90,000 psi, one failure
8. = 90,000 psi, two failure, 2.1 mm apart in the same fiber
9. = 120,000 psi, one failure
10. = 120,000 psi, two failures, 2 mm apart in the same fiber

Fig. 11 and 12. Fiber failures within the composite in broken parts resulting from composite failure. These fractographs show the effect of the etching process on the tungsten core.

Fig. 13. Typical fracture distributions along the gage length.

Fig. 14. Number of breaks per unit length versus load at fracture.

Fig. 15 to 17. Fractographs corresponding to long broken parts (6, 5 and 5.7 cm respectively).

Fig. 18 and 19. Fractographs corresponding to short broken parts (2 and 5 mm respectively).

Fig. 20 to 22. Fractures produced by bending the specimens by hand.

Fig. 23 to 26. Fractographs showing longitudinal crack propagation along the fibers.

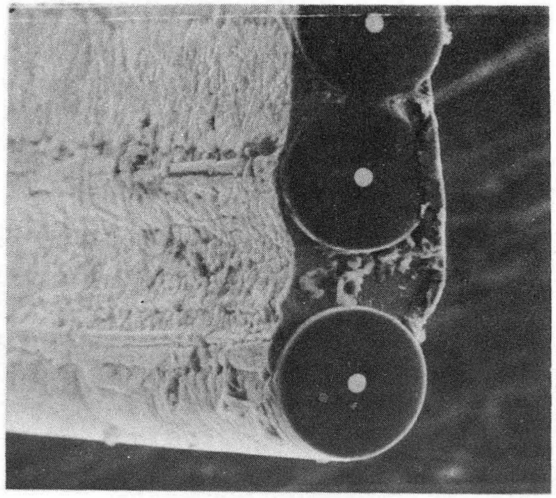

Fig. 1.

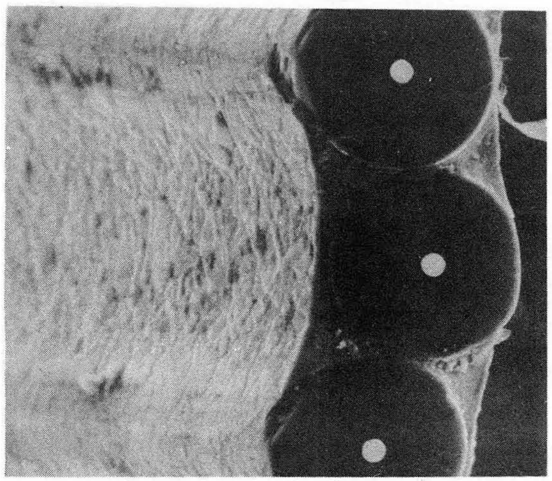

XBB 718-3572

Fig. 2.

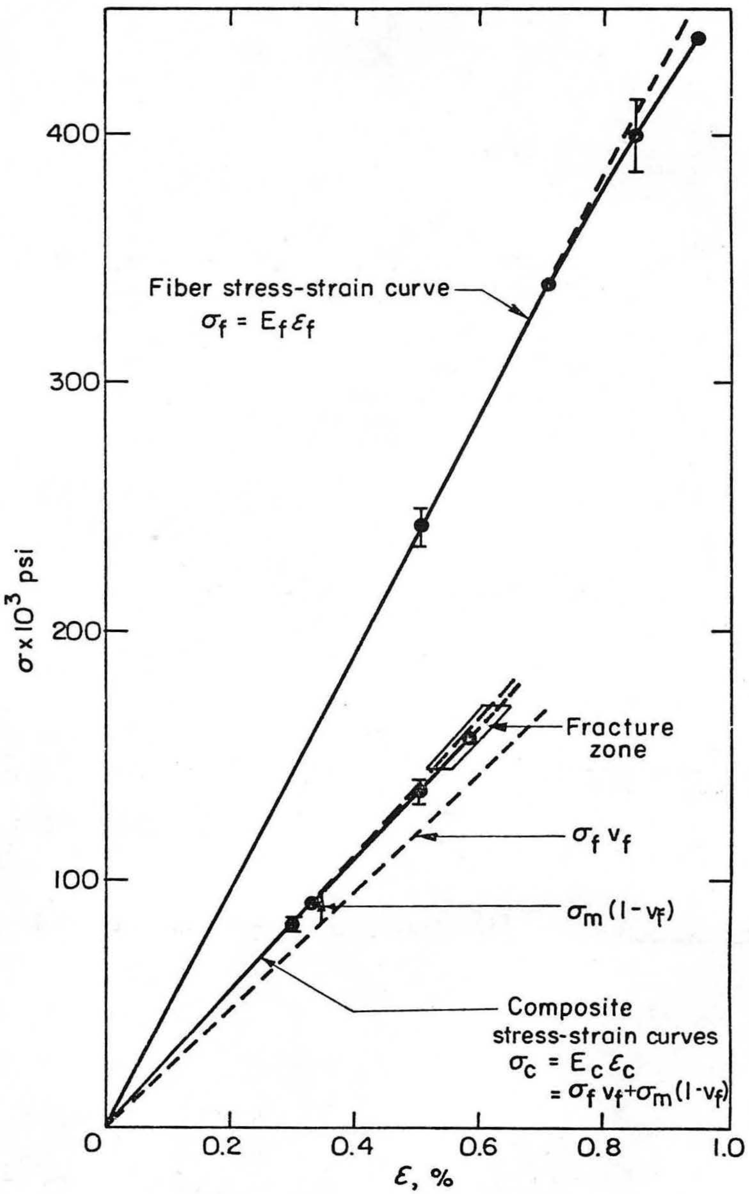

XBL717-7079

Fig. 3.

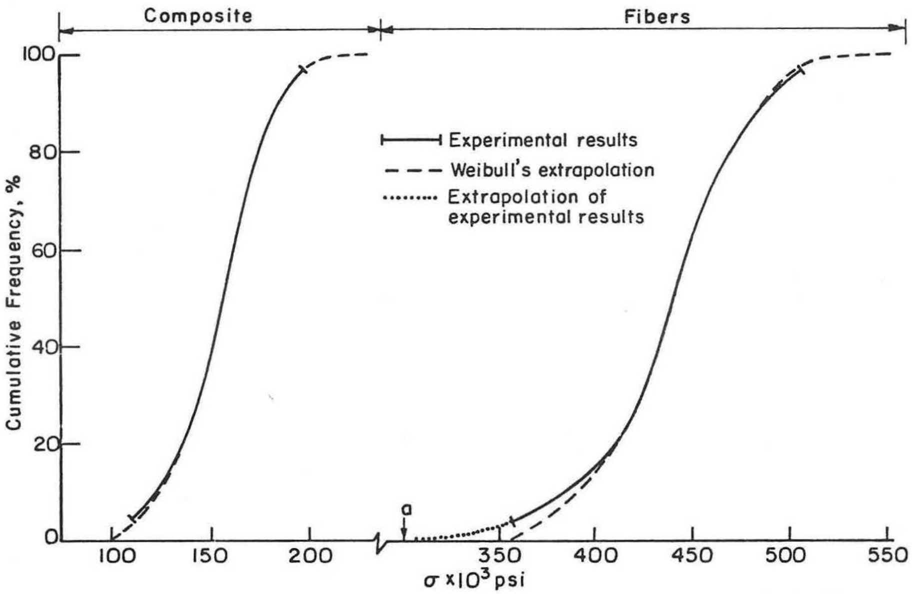

Fig. 4.

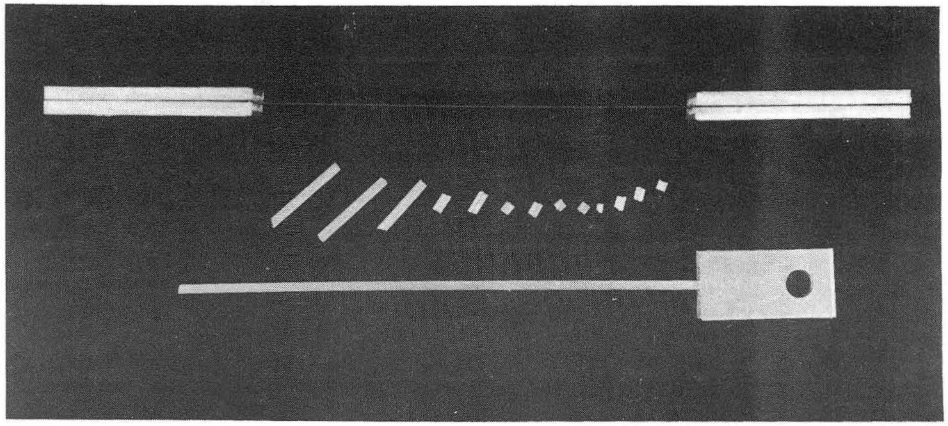

XBB 718-3768

Fig. 5.

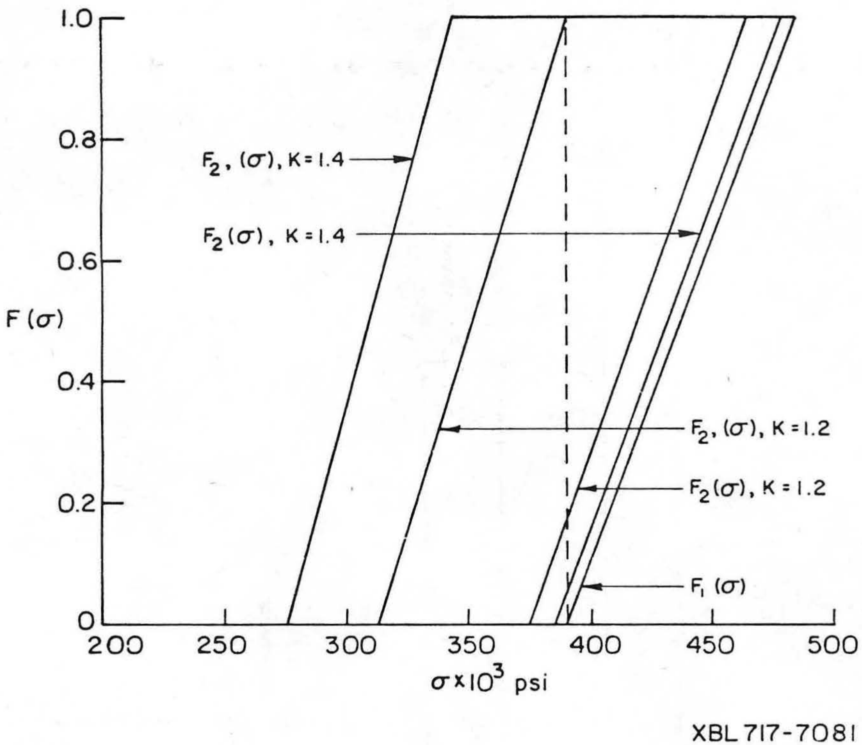

Fig. 6.

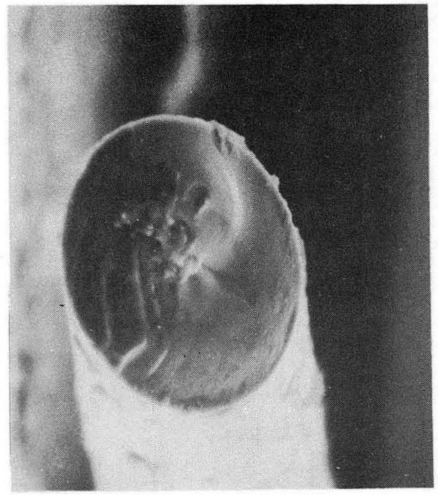

Fig. 7.

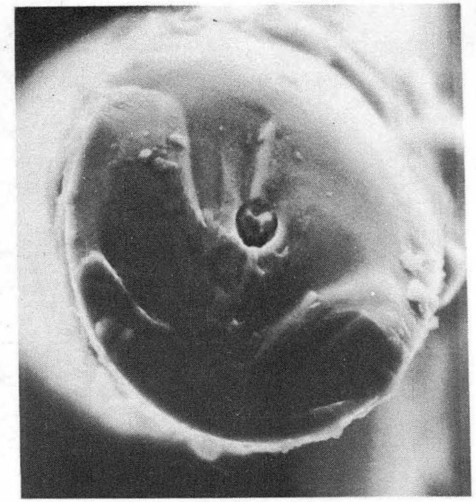

Fig. 8.

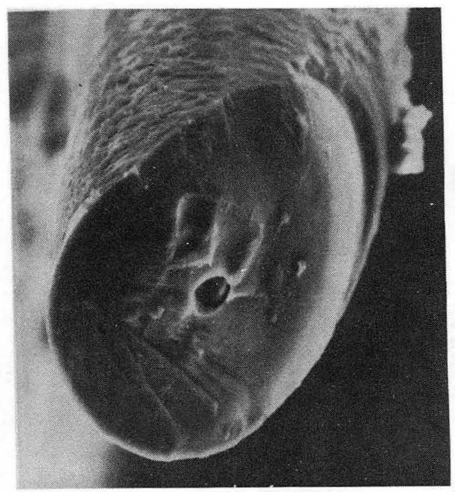

Fig. 9.

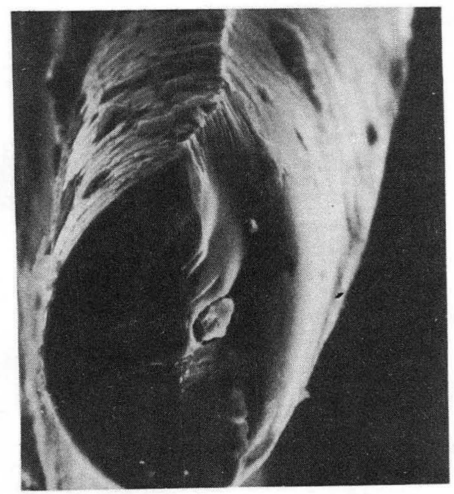

XBB 718-3574

Fig. 10

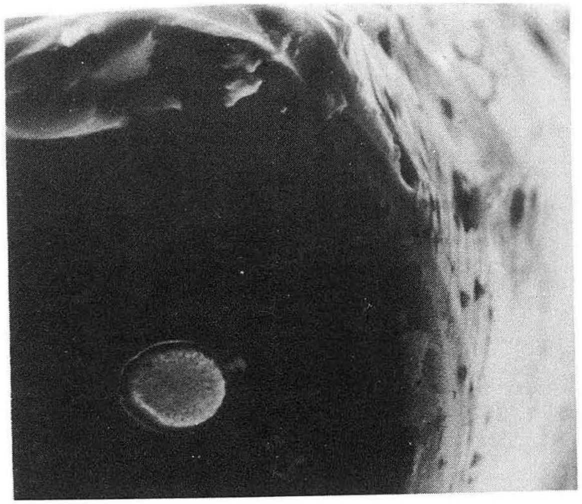

Fig. 11.

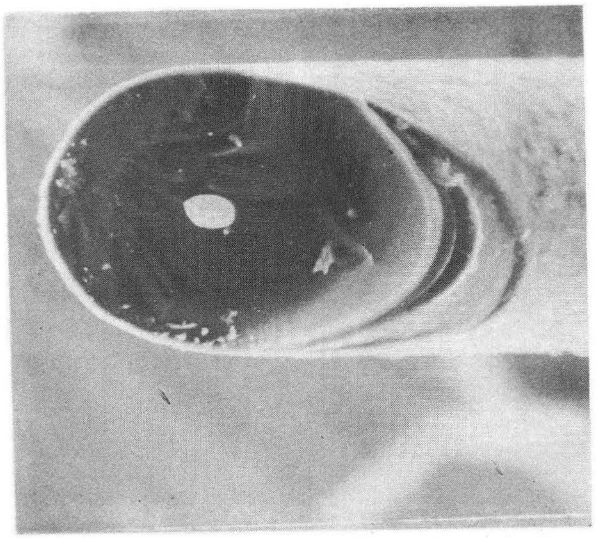

XBB 718-3577

Fig. 12

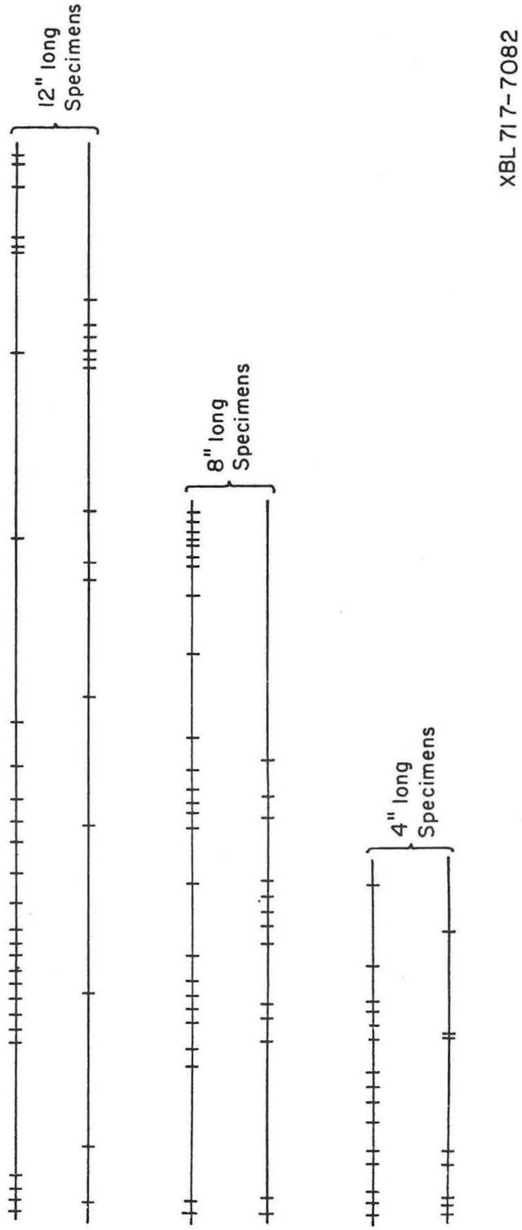

Fig. 13.

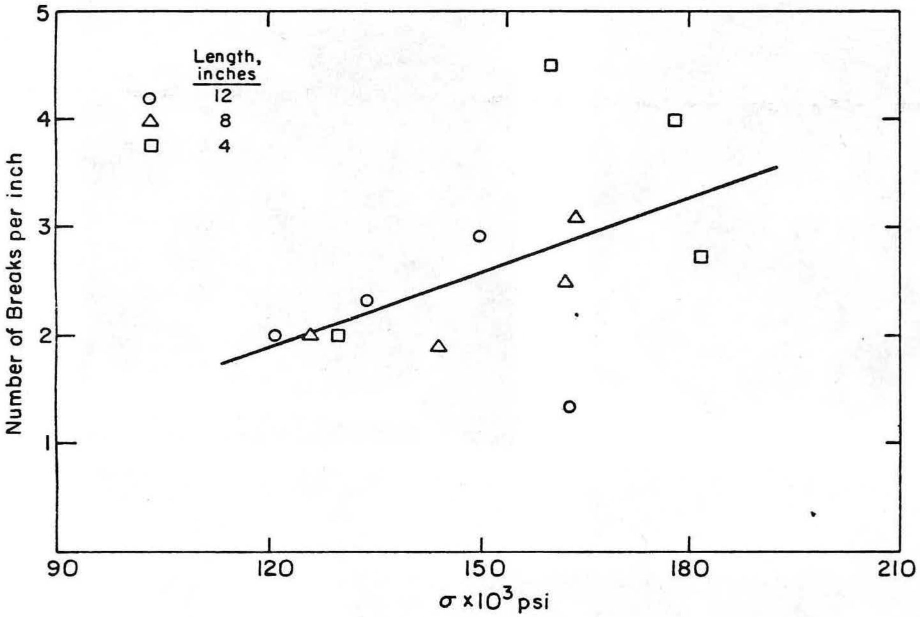

XBL 717-7083

Fig. 14.

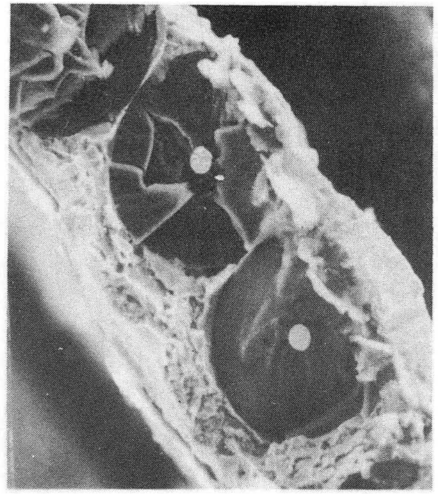

Fig. 15.

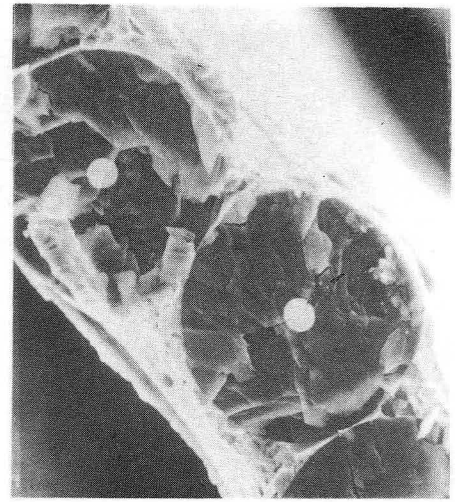

Fig. 16

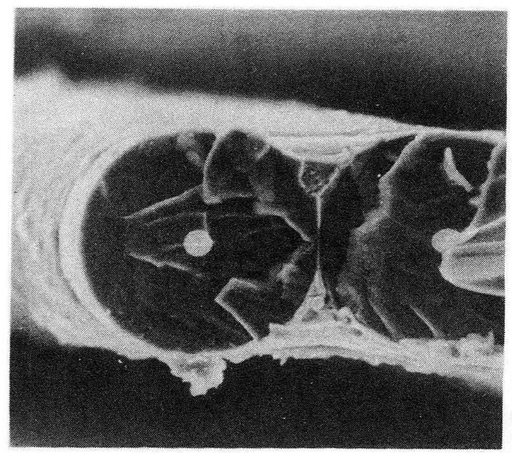

XBB 718-3578

Fig. 17.

TECHNICAL INFORMATION DIVISION
LAWRENCE BERKELEY LABORATORY
UNIVERSITY OF CALIFORNIA
BERKELEY, CALIFORNIA 94720